Mon. Not. R. Astron. Soc. **424,** 789–799 (2012) doi:10.1111/j.1365-2966.2012.21283.x

Time-dependent simulations of emission from the FSRQ PKS 1510−089: multiwavelength variability of external Compton and synchrotron self-Compton models

Xuhui Chen,[1⋆] Giovanni Fossati,[1⋆] Markus Böttcher[2] and Edison Liang[1]

[1]*Department of Physics and Astronomy, Rice University, Houston, TX 77005, USA*
[2]*Astrophysical Institute, Department of Physics and Astronomy, Ohio University, Athens, OH 45701, USA*

Accepted 2012 May 9. Received 2012 May 8; in original form 2012 March 31

ABSTRACT

We present results of modelling the broad-band spectral energy distribution (SED) and multiwavelength variability of the bright flat spectrum radio quasars PKS 1510−089 with our time-dependent multizone Monte Carlo/Fokker–Planck code. As the primary source of seed photons for inverse Compton scattering, we consider radiation from the broad-line region (BLR), from the hot dust of the molecular torus and the local synchrotron radiation [synchrotron self-Compton (SSC)]. We evaluate the viability of different Compton models by comparing simulated multiwavelength light curves and SEDs with one of the best observed flares by PKS 1510−089, in 2009 March. The time dependence of our code and its correct handling of light travel time effects allow us to fully take into account the effect of the finite size of the active region, and in turn to fully exploit the information carried by time-resolved observed SEDs that are becoming increasingly available since the launch of *Fermi*. We confirm that the spectrum adopted for the external radiation field has an important impact on the modelling of the SED, in particular for the lower energy end of the Compton component which is observed in the X-ray band, which in turn is one of the most critical bands to assess the differences between external Compton and SSC emission. In the context of the scenario presented in this paper, where the flaring is caused by the increase of the number of relativistic electrons ascribed to the effect of the interaction of a portion of the jet (blob) with a shock, we cannot firmly discriminate the three main scenarios for γ-ray emission. However, results show clearly the differences produced by a more realistic treatment of the emitting source in the shape of SEDs and their time variability over relevant, observable time-scales, and demonstrate the crucial importance of time-dependent multizone models to advance our understanding of the physics of these sources, by taking full advantage of the wealth of information offered by the high-quality data of current multiwavelength campaigns.

Key words: radiation mechanisms: non-thermal – methods: numerical – galaxies: active – galaxies: jets – quasars: individual: PKS 1510-089.

1 INTRODUCTION

The spectral energy distributions (SEDs) of blazars usually show two major non-thermal components. The low-energy one, peaking in the infrared (IR)–optical–X-ray range, is identified as synchrotron radiation. The origin of the high-energy one, peaking in the γ-ray energy range (MeV–TeV), is less clear. Proposed ideas include leptonic models, based on inverse Compton (IC) scattering by the same electrons emitting the synchrotron radiation, and hadronic models, in which protons play a critical role in producing the high-energy emission (Mannheim 1998; Rachen 2000; Sikora & Madejski 2001; Arbeiter, Pohl & Schlickeiser 2005; Levinson 2006; Böttcher 2007; Dermer & Lott 2012).

For the leptonic IC-based models, several sources of the target photons are possible and the debate about which one is dominant and in which type of object has recently been reignited. If the seed photons are provided by the synchrotron radiation emitted at lower energy by the same IC-scattering electrons, it is referred to as synchrotron self-Compton (SSC). Scenarios in which the dominant

⋆E-mail: xuhui.chen@alumni.rice.edu (XC); gfossati@rice.edu (GF)

contribution to the seed soft photon field for IC is provided by radiation emitted elsewhere are referred to as external Compton (EC) models. External sources of seed photons may include the photons from accretion disc, hot X-ray-emitting corona, broad emission line region, IR torus, host galaxy bulge and cosmic background radiation (Ghisellini & Tavecchio 2009).

There are two major classes of blazars: BL Lac objects, which have featureless optical spectra, and flat spectrum radio quasars (FSRQs), which exhibit broad quasar-like emission lines. The presence of these latter in FSRQs suggests that their jets are in an environment with a stronger external radiation field. Furthermore, depending on the relative location of these sources external to the jet and of active jet region (blob), the emission from the external sources would be relativistically beamed and enhanced in the frame of the blob, possibly making them dominant over the locally produced synchrotron emission. Therefore, the EC model is frequently invoked to explain the emission of FSRQs (Dermer, Schlickeiser & Mastichiadis 1992; Sikora, Begelman & Rees 1994; Sikora et al. 2009).

A major defining feature of blazars is their rapid and large variability, observed over the entire range of their continuum emission (radio–TeV γ-rays). Simultaneous multiwavelength observations and the correlation analysis of the observed multiwavelength variability can provide insights to the physics of particle processes and radiation mechanisms in the jet. The detailed observation and modelling of such variability have been performed extensively for high-energy-peaked BL Lacs (HBLs) such as Mrk 421 (Fossati et al. 2008; Chen et al. 2011b) and PKS 2155−304 (Aharonian et al. 2007; Katarzyński et al. 2008).

In the case of HBLs, such studies are facilitated by their synchrotron SED peak falling in the X-ray range which can be observed with multiple X-ray satellites, while their high-energy SED peak in TeV γ-ray is covered by ground-based Atmospheric Cherenkov Telescopes (for a review, see Hinton & Hofmann 2009; for examples of Mrk 421, see Fossati et al. 2008; Abramowski et al. 2012).

The launch of *Fermi* has re-opened the GeV γ-ray sky with unprecedented sensitivity and daily coverage. This energy band covers a highly variable part of the SED right above the peak of the high-energy component of the SED of several bright FSRQs, such as PKS 1510−089 (Abdo et al. 2010c) and 3C 454.3 (Abdo et al. 2009). Simultaneous coverage in other wavelengths such as optical and X-rays provided us a chance to obtain multi-epoch SEDs and cross-band correlations. A deeper understanding of these time series data sets requires time-dependent modelling with all light travel time effects (LTTEs) taken into account.

The importance of the LTTE in the study of blazars has long been realized (Chiaberge & Ghisellini 1999). The observed change of flux level on time-scale of hours in some blazars indicates that these effects must have a large impact on the variability of blazars. There have been some efforts to include these effects in the modelling of blazars (Kataoka et al. 2000; Sokolov, Marscher & McHardy 2004; Sokolov & Marscher 2005; Graff et al. 2008; Katarzyński et al. 2008), but none of them has taken into account all of these effects in a generic 2D geometry.

We have developed a time-dependent multizone code using the Monte Carlo method for radiation transport and the Fokker–Planck equation for electron evolution, which we first applied to a study of the correlated X-ray/γ-ray variability of the HBL Mrk 421 using a pure SSC model (Chen et al. 2011b).

In this paper we extend the model to include external sources of IC seed photons and apply it to study the multiwavelength variability of an archetypical powerful FSRQ, PKS 1510−089.

2 PKS 1510−089

PKS 1510−089 is a FSRQ at a redshift of $z = 0.361$ (Thompson, Djorgovski & de Carvalho 1990). It is one of the brightest and most variable sources detected by *Fermi*/Large Area Telescope (LAT). A feature that can be interpreted as disc emission [big blue bump (BBB)] is clearly visible in its optical/ultraviolet (UV) spectrum. Very long baseline interferometry observations of its jet show superluminal motion with apparent speed up to $45c$ ($\langle\Gamma\rangle = 36$; Jorstad et al. 2005).

Since the advent of *Fermi*, the long-term multiwavelength monitoring effort, complemented by more intense campaigns motivated by flaring phases, has lead to the observation of several large correlated flares for PKS 1510−089 (Kataoka et al. 2008; Pucella et al. 2008; Abdo et al. 2010b,c; Marscher et al. 2010; D'Ammando et al. 2011).

As reference data for our simulation we choose the observations of a high state observed in 2008–2009 and presented by Abdo et al. (2010c), D'Ammando et al. (2011) and Marscher et al. (2010). One particular flare at the end of 2009 March (peaking around March 25, MJD 54917) is chosen as the benchmark for this study.

We aim to reproduce several observational features by matching both the simulated light curves and SED with the observed ones. These features include the following.

(i) Clear presence of BBB emission with the general two non-thermal continuum components SED. The BBB is evident in both the high and the low states of the jet non-thermal continuum emission.

(ii) The time-scale of the flares, which were typically about 4 days (300 ks) at all wavelengths.

(iii) IR and γ-ray light curves show the stronger variations among the observed bands, with similar amplitude, up to a factor of 10. In the 2009 March flare, the IR (*R* band) and γ-ray (*Fermi*/LAT) fluxes were strongly correlated, with no significant lags.

(iv) The variations in the *Swift* Ultraviolet/Optical Telescope (*Swift*/UVOT) bands were less prominent than those in the IR–optical bands. The optical/UV spectral shape became softer when the source brightness increased, consistent with the combination of a variable softer broad-band continuum (synchrotron) and a non-variable component peaked in the UV band (BBB).

(v) The variability in the X-ray band luminosity was modest, within a factor of 2 over a period of 4 months encompassing the flare that we selected for this study [*Swift*/X-Ray Telescope (XRT) in Abdo et al. 2010c; *Rossi X-Ray Timing Explorer (RXTE)*/PCA in Marscher et al. 2010]. The spectrum was always very hard, with *energy* index $\alpha_X < 0.6$ ($F_\nu \propto \nu^{-\alpha}$) with very little variability. During the period around the benchmark flare it remained $\alpha_X \simeq 0.5$ (Abdo et al. 2010c).

(vi) The >0.2 GeV spectral shape as measured by *Fermi*/LAT did not vary significantly through large luminosity changes, remaining around $\alpha_\gamma \simeq 1.5$ (for a power-law fit) (Abdo et al. 2010c).

These characteristics only coarsely summarize the true richness of information provided by the full multiwavelength and multi-epoch data set which thanks to our simulations we can try to exploit more deeply. Nevertheless, they constitute a quicker and easier way of guiding the set-up and evaluation of the simulations and we will refer to them when discussing the comparison of our simulation results with observations in the following sections.

3 SIMULATIONS

3.1 Basic set-up and model parameters

Details and technical aspects of our Monte Carlo/Fokker–Planck code are described in Chen et al. (2011b, Chen 2012; Chen et al., in preparation).

The code uses the Monte Carlo method to track the production, travel and Compton scattering of photons, while it solves the isotropic Fokker–Planck equation to follow the evolution of electrons. The major strength and unique feature of this code are that it takes into account all the LTTEs, internal to the source volume (e.g. important for IC emission) and external, i.e. their effect on the observed radiation which we will receive at different times depending on where it was emitted in the source.

We model a jet active region (blob) as a cylindrical volume crossing a standing 'shock' as illustrated in Fig. 1. In the blob rest frame, where all calculations are performed, the shock moves through the cylindrical region with a speed equal to the bulk velocity of the blob $v_{\rm bulk} \sim c$. The cylindrical volume is divided evenly into zones in the radial and vertical directions (r and z coordinates, n_r, n_z). In all runs presented in this paper, $n_r = 9$ and $n_z = 30$.

At this stage the meaning of this shock is simply that of an agent affecting the properties of the simulation zone where it is at a given time. In the simulations presented in this paper it affects the electron distribution, namely it injects high-energy particles into the zones it currently resides in. It does not affect the magnetic field, which is assumed to be homogeneous throughout the volume and non-varying. The shock has not thickness (however, our resolution is limited by dz) and is treated as a surface perpendicular to the z-direction.

With respect to the simulations presented in Chen et al. (2011b), we added a few features to the code. The most relevant ones are

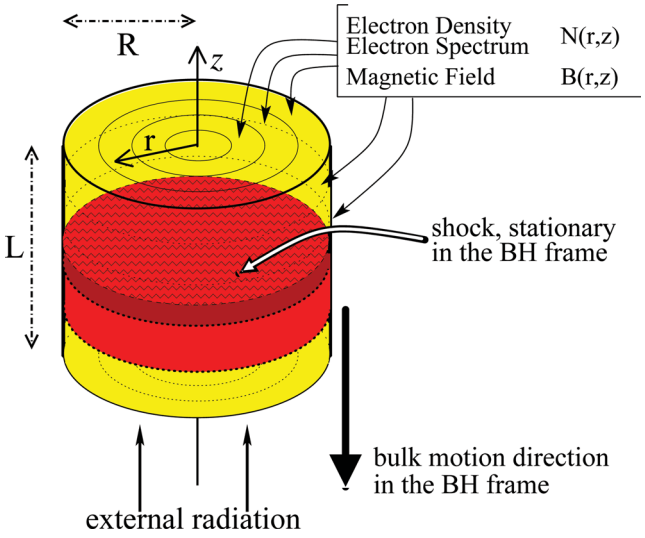

Figure 1. The geometry of the model. The volume is divided in the r and z directions in zones with their own electron distribution and magnetic field. We also schematically show the set-up for the variability of the simulations with a shock. The hatched layer represents a stationary shock. The blob moves downwards and crosses the shock front. For illustration purposes, we plot in lighter colour shade the zones that crossed the shock at earlier times and have had some time to radiate the newly injected energy. In this representation the photons from the external radiation fields, beamed in the blob rest frame, enter the blob from the bottom surface.

the inclusion of a spatially diffuse stochastic acceleration process, similar to the one discussed by Katarzyński et al. (2006), of a particle escape term and of a particle 'pick-up' term (see also Tramacere, Massaro & Taylor 2011).

These developments and their motivation are discussed in Chen et al. (2011a), Chen (2012) and Chen et al. (in preparation). We treat stochastic acceleration in the whole blob as a diffusive term in the Fokker–Planck equation, while the putative first-order Fermi acceleration at the shock front is simplified as directly injecting high-energy particles with a power-law distribution into the zones where the shock is present.

The main parameters of the model are (see also Table 1) as follows.

(i) Γ, the bulk Lorentz factor of the jet.
(ii) R and Z, the radius and height of the cylindrical simulation region.
(iii) B, the magnetic field strength, assumed here to be homogeneous and non-variable.
(iv) $n_{\rm e}$, the initial electron number density.
(v) $t'_{\rm acc}$ and $t'_{\rm esc}$, the time-scales parametrizing the stochastic diffuse acceleration and particle escape.
(vi) $Q_{\rm pick}$, the rate at which the blob constantly picks up mildly relativistic electrons (with a narrow Gaussian distribution centred at $\gamma_{\rm pick}$.
(vii) $L'_{\rm inj}$, the luminosity of the relativistic electrons injected by the shock.
(viii) $p_{\rm inj}$, $\gamma_{\rm min,inj}$ and $\gamma_{\rm max,inj}$ are the spectral index, minimum and maximum Lorentz factors of the electrons injected locally by the shock with a power-law spectrum.
(ix) $R_{\rm BLR}$ and $f_{\rm BLR}$ are the size of the broad-line region, assumed to be spherical and the fraction of the luminosity from the accretion disc that contributes to the radiation energy density within its volume. $R_{\rm IR}$ and $f_{\rm IR}$ are the corresponding parameters for the case of the IR-emitting torus. Collectively we also call them $R_{\rm ext}$ and $f_{\rm ext}$ without distinction between BLR and IR. We will discuss them in the following sections.

At the beginning of a simulation each zone of the blob is filled with electrons with density $n_{\rm e}$ and a power-law spectrum with slope and energy range given by p, $\gamma_{\rm min}$ and $\gamma_{\rm max}$. The same parameters are used in every zone. These parameters are not listed in Table 1 because their relevance is minimal; they are simply seeding each zone with electrons at beginning of the simulation, and they do not represent the electron distribution once the simulations starts.

The actual electrons distribution in each zone will be different from the seeded one, and from zone to zone, as they evolve separately. In the steady state it would approximate a power-law-like distribution, with $\gamma_{\rm min}$ determined by the energy of the picked-up electrons. The spectral index is related to $t'_{\rm acc}$ and $t'_{\rm esc}$, with faster escape and slower acceleration generally leading to softer spectrum. The $\gamma_{\rm max}$ is determined by the competition between acceleration and cooling, with faster cooling meaning smaller maximum electron energy.

3.2 External radiation

The relativistic jets in active galactic nuclei (AGN) may reside in dense external radiation environments, with contributions from the BLR (Tavecchio & Ghisellini 2008; Poutanen & Stern 2010) or the warm dust of the molecular torus hypothesized to exist beyond the accretion disc (Malmrose et al. 2011). For a thorough discussion we refer the reader to Ghisellini & Tavecchio (2009).

Table 1. Summary of model parameters.

Parameter	nf/blr	blr15	blr15highgmin	blr25	torus15	ssc
Jet bulk Lorentz factor, Γ	15.0	15.0	15.0	25.0	15.0	10.0
Z ($\times 10^{16}$ cm)	8.0	8.0	8.0	13.33	8.0	5.0
R ($\times 10^{16}$ cm)	6.0	6.0	6.0	10.0	6.0	3.75
Magnetic field, B	0.3	0.3	0.3	0.16	0.2	0.1
Particle density (initial), n_e ($\times 10^4$ cm^{-3})	2.66	2.66	2.66	0.14	7.37×10^{-2}	0.01
Particle escape time-scale, t'_{esc} (Z/c)	0.1	0.1	0.1	0.1	0.015	0.03
Particle (diffuse) acceleration time-scale, t'_{acc} (Z/c)	0.55	0.55	0.55	0.55	0.09	0.19
Electron pick-up rate, Q_{pick} (cm^{-3} s^{-1})	0.1	0.1	0.1	3.2×10^{-3}	0.0191	0.002
Pick-up electrons energy, γ_{pick}	5.0	5.0	5.0	5.0	50.0	1200.0
Shock injection: $\gamma_{min,inj}$	–	30	90	6	300	2000
Shock injection: $\gamma_{max,inj}$	–	2×10^4	2×10^4	4×10^3	2×10^5	10^5
Shock injection: power-law slope, p_{inj}	–	3.2	3.2	3.2	3.2	3.2
Shock injection: rate: L'_{inj} ($\times 10^{44}$ erg s^{-1})	–	3.5	2.0	2.8	5.0	8.0
R_{BLR} or R_{IR} ($\times 10^{18}$ cm)	0.8	0.8	0.8	0.8	7.8	–
f_{BLR} or f_{IR}	0.013	0.013	0.013	0.0015	0.5	–

The dominance of different sources of external radiation is connected to the location of the γ-ray-emitting region within the jets. The radiation from the BLR can be dominant only when the emission region is located at subparsec distance from the central engine of the AGN. Beyond that distance, the IR radiation from the dust torus is likely to dominate on parsec scale (Ghisellini & Tavecchio 2009). Poutanen & Stern (2010) argue that the GeV spectral breaks of FSRQs observed by *Fermi*/LAT are a sign of γ-ray absorption inside the BLR.

Meanwhile, Marscher et al. (2010) used the correlation between radio knot appearance and γ-ray flares to identify the location of the emission region at several parsecs from the central engine. We will test the viability of both of these two sources of external photons, and see if they can produce the SEDs and light curves observed.

We regard the BBB clearly visible in the SED of PKS 1510−089 when in its lower brightness states as unbeamed thermal emission from the accretion disc, and match the data with a luminosity of 4×10^{45} erg s^{-1} and a temperature of 3×10^4 K.

This disc emission is used to estimate the energy density experienced in the blob rest frame, while its location is within the radius of BLR, R_{BLR}, according to the following transformation equation (Ghisellini & Madau 1996):

$$U'_{BLR} \sim \frac{17}{12} \frac{f_{BLR} L_d \Gamma^2}{4\pi R_{BLR}^2 c}, \quad (1)$$

where L_d is the disc luminosity.

Similarly, assuming for simplicity that the region where radiation from the dusty torus yields a significant energy density can be described as a spherical volume of radius R_{IR}, the energy density within this region as seen in the blob rest frame can be estimated by

$$U'_{IR} \sim \frac{f_{IR} L_d \Gamma^2}{4\pi R_{IR}^2 c} \quad (2)$$

(Ghisellini & Tavecchio 2009).

For the spectrum of BLR emission, we consider two cases: an approximation as a plain single-temperature blackbody peaked at $1.5\Gamma\nu_{Ly\alpha}$ or a more realistic spectrum obtained by taking the unbeamed BLR spectrum in fig. 4 of Tavecchio & Ghisellini (2008) and beam it according to the equation:

$$U'(\nu') = \frac{2\pi}{\Gamma\beta c}\nu'^2 \int_{\nu_1}^{\nu_2} \frac{I(\nu)}{\nu^3} d\nu, \quad (3)$$

here $\nu_1 = \nu'/[\Gamma(1+\beta)]$, $\nu_2 = \nu'/\Gamma$, $I(\nu)$ is the unbeamed intensity spectrum, and ν and ν' are the frequency in the observer's frame and blob frame, respectively.

For the IR emission from the hot dusty torus, we use a blackbody spectrum with temperature (Ghisellini & Tavecchio 2009):

$$T'_{IR} = 370\ \Gamma\ (1 - \beta\cos\alpha)\mathrm{K} \sim 370\,\Gamma\mathrm{K}, \quad (4)$$

where α is the angle between the jet axis and the line connecting the source and the jet, so $\alpha \sim \pi/2$ for the torus.

For computational ease, we simplify the model by assuming that all the external photons are travelling in the upward direction in the frame of the blob, as illustrated in Fig. 1. All the external photons enter the blob through the lower boundary and the external flux is just the energy density times c. This is a valid approximation for the typical (large) values of the Lorentz factor appropriate for blazars, which we adopt for ease of computation, although our code allows us to set up the flux from the external illuminating source with an angular distribution.

To produce the observed SEDs the disc emission is added as a non-varying component to the beamed emission from the jet in the post-processing of the simulation results.

3.3 About model parameters freedom and constraints

In the EC models, we have five basic observables (variability time-scale τ_{var}, synchrotron luminosity L_{sync}, estimated IC peak frequency $\nu_{IC,p}$, IC luminosity L_{IC} and γ-ray spectral index α_γ) to constrain six free parameters (R, B, n_e, f_{ext}, γ_{min} and p_{inj}). However, there are in fact additional constraints available to further limit the usable range of parameter space. For example, as we will discuss later, in the EC cases the SSC flux cannot be too high in order to be consistent with the moderate X-ray variability, which in turn translates into a requirement on the magnetic field strength to be sufficiently large. On the other hand, the required diffuse stochastic acceleration time-scale (t'_{acc}) and hence the cooling time-scale cannot be too short, which then imposes a limit on how large the magnetic field can be.

Moreover, as already noted, the value of p and γ_{max} in the quiescent state are not direct input parameters. They are the results of the combination of t'_{acc} and t'_{esc} (and the relevant cooling time-scale). The synchrotron peak frequency $\nu_{sync,p}$ is not always used as a

constraint because for the physical conditions of our simulations it is not a result of the electron distribution, but it is often determined by synchrotron self-absorption. At the same time, observationally its position in the SED is only poorly constrained by currently available data.

For some other parameters, such as the bulk Lorentz factor of the jet, the radius of the BLR or torus regions, values are set on the basis of empirical estimates obtained by independent studies and therefore may not be regarded as truly free parameters. On the other hand, because the energy density of the external radiation in the blob frame, $U'_{\rm ext} \sim f_{\rm ext}\,\Gamma^2/R^2_{\rm ext}$ and $L_{\rm EC}/L_{\rm sync} \sim U'_{\rm ext}/B^2$, a given SED or set of SEDs will impose a relationship between these parameters.

The size scales of BLR and torus are generally found to follow a relationship like $R \sim L^{1/2}_{\rm disc}$, with some range in the normalization typically yielding a $R_{\rm BLR}=$ few $\times\,10^{17}$ cm and $R_{\rm IR}=$ few $\times\,10^{18}$ cm for a disc luminosity of the order of that inferred in PKS 1510−089 on the basis of the observed BBB. We thus decided to set $R_{\rm ext}$ to the value closed to the ones expected from these estimates and given the uncertainty on the $f_{\rm ext}$ to regard its value as a free parameter controlling the normalization of the EC emission.

4 RESULTS

As illustrated in Section 2 our aim is to reproduce the quiescent and flaring states of PKS 1510−089.

We model a flare as being caused by an injection of relativistic electrons ascribed to the effect of the interaction of the blob with a standing shock, as described in Section 3.1. As the shock travels through the blob (in the blob frame) it injects new particles locally, i.e. in the zones where it currently resides. These newly injected electrons are treated in the same way as all other electrons in each zone; they radiate through synchrotron and IC, and evolve according to the same Fokker–Planck equation.

We will review cases with BLR or torus as the dominant sources of external photons for EC, as well as a pure SSC model, and compare light curves and SEDs with those of the 2009 March observations of PKS 1510−089.

In discussing the comparison we will mainly focus on the SEDs, in particular on the IR, X-ray and γ-ray bands. The light curves, which we show for several observable bands, provided an important constraint guiding the analysis and identifying suitable parameter values but they do not illustrate the differences between different cases as clearly as the comparison of data and SEDs for multiple epochs. This is also due to the fact that purely in terms of intensity variation in narrow bands, the longest time-scale dominates (modulates) the time profile of a flare, and in the cases discussed here the source crossing time is larger than time-scales for electron processes.

This was not true for instance for Mrk 421, for which as shown in Chen et al. (2011b) the light-curve profiles for various X-ray and TeV bands were different depending on whether the particle related time-scales were faster or slower than the source crossing time, providing us with additional diagnostics.

4.1 Quiescent state: no shock

First we try to reproduce the quiescent-state SED using as reference the period of the last 3 months of 2008 during which the γ-ray flux measured by *Fermi*/LAT remained low and with small variations (the 'quiescent' period in the naming adopted in Abdo et al. 2010c).

We begin with using the blackbody approximation for the spectrum of the BLR emission. We show the results of this simulation in Fig. 2, with the parameters used listed in Table 1.

In this simulation particle injection is exclusively given by the steady-state pick-up term $Q_{\rm pick}$. Because there is no flaring activity, the flux level at every wavelength reaches the steady state after a few light crossing times, and the light curves remain almost flat except for statistical fluctuations.

It is interesting to note that the *R*-band light curve reaches a flux level higher than the quiescent level before it reaches steady state (effect noticeable also in the SED in the IR band). This is

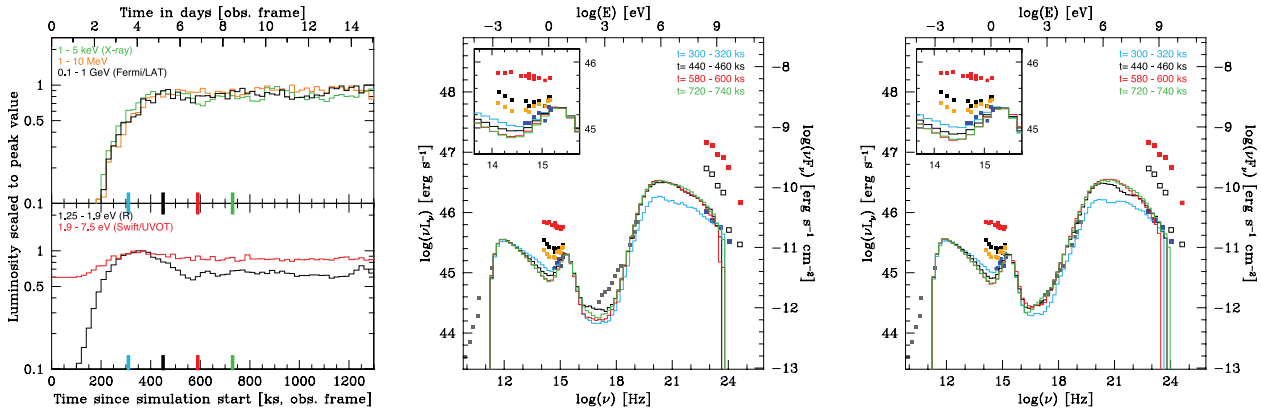

Figure 2. Left, middle: light curves and SEDs for the quiescent state of the EC/BLR model, using a blackbody approximation for the BLR spectrum. The histograms in both figures are the results of our simulation, with the energy band chosen shown in the legend of the left figure. The SED snapshots times are shown in legend of figures and marked with matching colour segments in the light-curve plot. In this and all the SED plots in this paper, the data points are multiwavelength SEDs of PKS 1510−089 mostly in the spring of 2009 from Abdo et al. (2010c) and D'Ammando et al. (2011). The optical/infrared points, also shown in the inset, are for the following dates: blue for March 10, orange for March 18, black for March 19 and red for Match 25/26 (flare peak). The γ-ray, *Fermi*/LAT spectra are as follows: blue squares for the quiescent state of the early 2009 (see Abdo et al. 2010c), red squares for the end of 2009 March flare and black empty squares for an earlier weaker flare (flare 'a' in Abdo et al. 2010c) which we show as a plausible reference for the gamma-ray state before and after the 2009 March flare. The grey points in radio, submm and X-ray are not strictly simultaneous but we regard them as representative because of the very modest variability exhibited by the source during those months in these bands. The X-ray data include the XRT data averaged during the 2009 March flare, and 5-year integrated BAT data in hard X-rays. Right: the SEDs for the quiescent state of the BLR model using the Tavecchio & Ghisellini (2008) BLR spectrum (parameters are listed in Table 1, `nf/blr`).

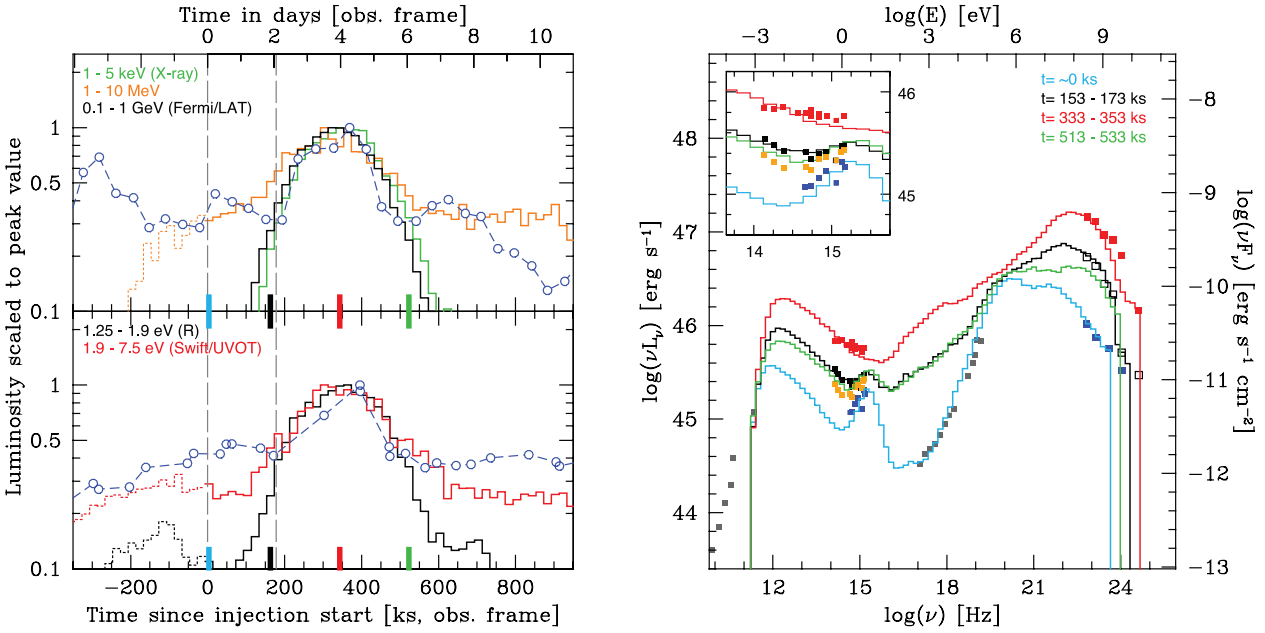

Figure 3. Light curves (left) and SEDs (right) for the first EC/BLR scenario. In these and all following light-curve plots the blue circles in the lower panel show the observed *R*-band light curve in 2009 March from the *GLAST-AGILE* Support Program (GASP), those in the upper panel show the *Fermi*/LAT light curve above 0.2 GeV in 2009 March, simultaneous with the *R*-band data (Abdo et al. 2010c). The SED data points are the same as those in Fig. 2. Simulation light curves are dotted before $T = 0$ to emphasize that interval should be regarded as a set-up time for the simulated region. The two grey vertical dashed lines mark the start and end of the injection time, i.e. the time during which the shock is crossing the blob. The SEDs correspond to the times (in the observer frame) given in the legend, and marked with coloured ticks in the light-curve plot. Model parameters are given in Table 1, `blr15`.

because the external photons need some time (of the order of 1 light crossing time) to diffuse through the whole blob.[1] During that time some zones which have not yet received the external photons will experience significantly less IC cooling (which is dominant over synchrotron cooling in this case). Hence the higher energy portion of their electron spectrum will remain at a relatively higher level and produce a relatively more intense synchrotron radiation during this phase. This is an example of how the LTTE can affect the actual physics in the jet, not only just the way we perceive the emission. While in this particular case the initial phase of the simulation and particle evolution is not of astrophysical interest, this effect is realistic and illustrates one important aspect of taking into account the finite size of the source and the effect of light travel time on the physical evolution of the system and its emission.

The SEDs match the low-state data points at optical and γ-ray frequencies pretty well. The radio data points do not match because it is likely that the radio emission comes from additional emission regions rather than just the one producing the optical and γ-ray emission. The simulated spectrum in the X-ray regime is much harder than the observed one. This improves significantly by using a more detailed description of the BLR spectrum such as that discussed by Tavecchio & Ghisellini (2008), as shown by the SEDs in Fig. 2, where we used a BLR spectrum obtained from their analysis. This confirms their conclusion that an accurate treatment of the BLR spectrum used for the EC emission is necessary in producing the spectrum in the soft to medium X-ray band (∼0.1–10 keV), where usually high-quality data are available. This band is of critical importance because it can provide constraints on the relative contribution of SSC and EC, and also on the characteristics of the lower energy end of the electron distribution.

[1] The same is true for the internally produced synchrotron photons scattered by SSC. Their contribution to the photon field in each location will need a time of the order of the light crossing time to stabilize, or, in the case of variable synchrotron emission, to respond to the changes of intensity happening elsewhere in the blob.

4.2 EC/BLR: shock crossing with $\Gamma = 15$

Starting from a baseline quiescent state like the one just discussed, we model the flare for a case in which the dominant EC contribution is from the BLR. For this first case we adopt a blob bulk Lorentz factor $\Gamma = 15$. The results are shown in Fig. 3.

Light curves show that the optical/IR variability is larger in the *R* band than in the bluer *Swift*/UVOT bands, due to the contribution of the non-variable BBB emission in the UV. This is consistent with observations.

Both the X-ray light curve and the SEDs clearly show that our simulations predict large-amplitude variations in the X-ray flux. This is at odds with observations which show only modest X-ray variability (less than a factor of 2) throughout the entire 2009 observing campaigns, including the largest flares. The excessive X-ray variation in our simulations is the result of SSC emission. Although currently our model does not track separately photons of EC and SSC origin, the parameters we use indicate that emission by SSC is not negligible in the X-ray band even in the quiescent state. In the case of a flare caused by changes in the electron spectrum and/or density, the amplitude of variation of the SSC emission will always be larger than that of the synchrotron (as long as we are considering electrons scattering in the Thomson regime, which is the case here). Therefore as we model the factor of 10 increase of the non-thermal emission in the optical/IR band the corresponding IC emission will vary by a factor up to a 100, with a large contribution in the X-ray band.

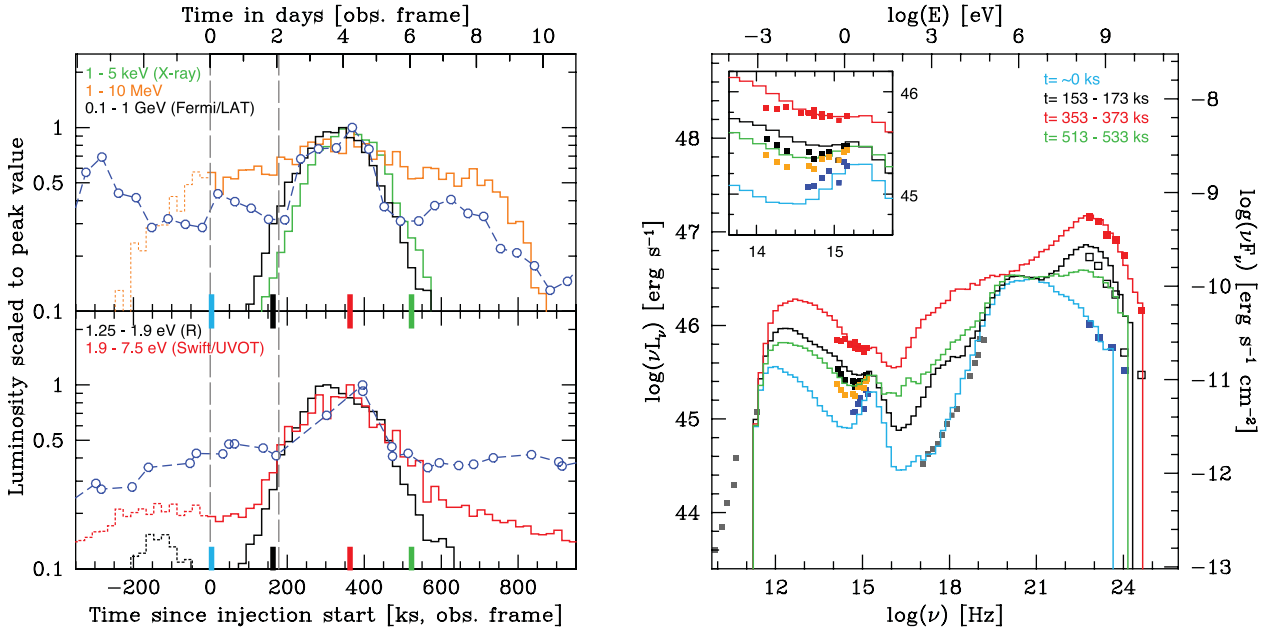

Figure 4. Same as Fig. 3 for the second case of EC/BLR flare simulations, with $\Gamma = 15$ and higher minimum energy for the injected electrons, $\gamma_{\rm min} = 90$ (see Table 1, `blr15highgmin`).

This SSC variation makes this model and parameter set not consistent with the observed features of PKS 1510−089.

This example also illustrates the importance of modelling the time evolution of the SED, rather than simply modelling with sets of parameters left fully free to vary between different epochs the high- and low-state SEDs, or even sequences of SEDs taken close enough in time during a single flare that they are very likely to be related to each other as part of the development of a single event.

4.2.1 Quiescent versus flaring state and the importance of time-dependent multizone modelling

The comparison between the SEDs of the steady and flaring states shown in Figs 2 and 3 illustrates another important difference between a time-dependent multizone simulation and a one-zone (effectively point-like) simulation, for which the quiescent case can be considered a proxy:[2] the SEDs of the more realistic model are significantly more complex in the shape and variation of the high-energy component. This is the result of both internal and external LTTEs giving to the observer a mix of emission produced at different times in zones at different stages of the flare development and with electron distributions at different stages of their evolution.

Even if locally the processes affecting the electrons are fast and the particle spectrum could be regarded as reaching rapidly a steady state (in the case of injection lasting for a long enough time), the sequence of SEDs produced in a flare is not equivalent to a sequence of steady-state SEDs (see Bonnoli et al. 2012, for an example of this approach applied to the FSRQ 3C 454.3).

Admittedly in this paper we are presenting one possible scenario for the flaring state of a FSRQ, but this type of differences can be expected to exist for a wide range of plausible scenarios of variable emission from a relativistic jet.

[2] The steady-state emission is effectively equivalent to what would be produced by a one-zone non-time-dependent code.

4.3 EC/BLR: $\Gamma = 15$, with higher $\gamma_{\rm min}$

A potential remedy for the excessive X-ray variability crisis could be to increase the minimum energy of the injected electrons. The peak of the emission of the variable component, driven by the electron injection, is determined by the electron's $\gamma_{\rm min}$. A higher $\gamma_{\rm min}$ may push the SSC emission by these electrons to peak at a higher frequency where it can be 'hidden' beneath the rapidly rising stronger EC emission. However, $\gamma_{\rm min}$ is fairly constrained by the observed MeV–GeV γ-ray spectrum, namely by the fact that we do not observe a spectral turnover in the *Fermi*/LAT data. Too large a $\gamma_{\rm min}$ will produce a EC SED peaking in the *Fermi*/LAT observational band. With this in mind, we tested one case with a slightly higher injected $\gamma_{\rm min} = 90$. The results are shown in Fig. 4.

The peak of the EC SED in this case is shifted close to the lowest energy data point of the *Fermi*/LAT spectrum, indicating that $\gamma_{\rm min} = 90$ is already of the order of the largest value that we can use with the current BLR spectrum and a Lorentz factor of 15. On the other hand, while there is some change on the spectral shape of the high-state X-ray spectra, the fundamental problem of the excessive amplitude of its variation is not mitigated. The inconsistency between the observed and simulated X-ray variability remains a problem in the higher injected $\gamma_{\rm min}$ case.

4.4 EC/BLR: higher Lorentz factor, $\Gamma = 25$

Instead of moving the SSC emission in frequency, another route to solve the X-ray variability inconsistency may be to decrease the level of the SSC emission relative to the other components. In order to do this while keeping the same level of synchrotron emission, we need to decrease the ratio between the synchrotron (SSC seed photons) energy density and the magnetic energy density. We can achieve this by increasing the Doppler factor because in that case the synchrotron energy density in the blob frame needs to decrease accordingly to match the optical data. This requires to change the values of other parameters to produce a SED well fitting

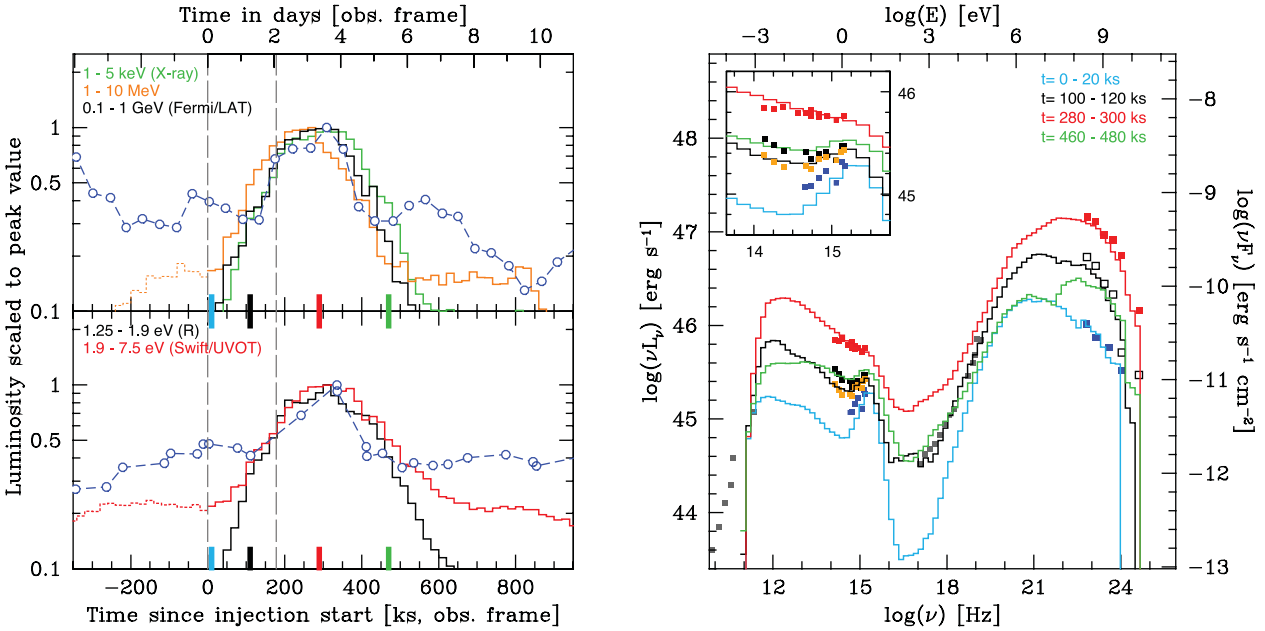

Figure 5. Light curves (left) and SEDs (right) for the EC/BLR case with higher bulk Lorentz factor, $\Gamma = 25$. Parameters are given in Table 1, `blr25`.

the observed one. The modified parameters are reported in Table 1. The results are shown in Fig. 5.

In this case, the luminosity in the X-ray dip between the two main components is indeed lower. Nevertheless because any SSC emission occurring in this band would still be varying by a factor larger than that of the optical flux, the range of the X-ray variation remains large, and easily exceeding the constraint set by the well-measured X-ray intensity and spectrum. However, since in this case the quiescent X-ray flux is lower than the observed one, it may be possible to explain the X-ray band spectrum as comprising a contribution from additional, relatively cooled blobs, which would partially dilute the large variation. However, even taking that into account, considering the spectral variability present in the varying X-ray component, it may not be straightforward to reconcile the overall X-ray properties with the remarkably stable observed spectra.

4.5 EC dominated by IR emission from the torus

Emission from hot dusty, molecular, gas in the putative torus surrounding the accretion disc is another plausible source of external photons in the immediate environment of the relativistic jet.

This scenario is motivated by the observation of the coincidence of γ-ray flares with the appearance of new knots in radio images of PKS 1510−089 (Marscher et al. 2010). These observations hint that the emission region responsible for γ-ray flares is located at parsec scales, which is beyond the usually inferred radius of the BLR (Bentz et al. 2006, 2009; Kaspi et al. 2007). At this distance, the IR torus (Pier & Krolik 1992a,b) becomes the main candidate as the source of EC seed photons (Ghisellini & Tavecchio 2009; Sikora et al. 2009).

We calculate the energy density and temperature of the torus emission according to equations (2) and (4).

Because the energy density and SEDs of the emission from the torus are very different from those of the BLR, it is necessary to change the values of several parameters to be able to match the quiescent and then flaring states. The best set of parameters is reported in Table 1, and the light curves and SEDs in Fig. 6.

The broad-band SEDs compare reasonably well with observations; the light curves vary on a time-scale consistent with the data; the optical and γ-ray light curves are well correlated with no significant lags; the variations in the optical and γ-ray bands have similar amplitude; the variations in the UV band are less prominent than those in the optical.

However, it is worth noting that it has proven to be difficult to concurrently match the GeV spectrum and the soft slope through the IR bands. Although we cannot claim to have achieved a perfect match in the latter in the previous cases, this is an issue that did not seem to emerge as seriously as here.

The problem of X-ray variability in this case is similar to the one in the BLR case. It is likely that similarly to the previous case, a higher Doppler factor would lower the flux produced by SSC in the X-ray band.

One of the main differences between the torus emission and the BLR emission as source of EC seed photons is that the owing to its lower temperature the torus radiates at lower frequency compared to the BLR. This means that to scatter these seed photons to the same γ-ray energies, the energy of the electrons needs to be higher than those needed in a BLR scenario. In the context of the scenario presented in this work, this means that more efficient particle acceleration is needed to sustain the high-energy electrons, which have faster cooling times. This also means that faster particle escape is to be expected in the torus scenario, otherwise the accelerated particles will not form a power-law distribution that can produce emission with the observed spectral shape. It turns out that the value for the particle escape time-scale parameter needed in this case may be too fast to be realistic ($t'_{\rm esc} = 0.015\, Z/c$).

However, it is worth emphasizing that, chosen name notwithstanding, the 'escape' term in the kinetic equation may be regarded as a crude approximation for describing a generic energy-independent process affecting electrons, and in this sense a value significantly smaller than the source crossing time may not be automatically be considered unphysical. Nevertheless, because the time-scale for plausible candidate such as actual escape or adiabatic cooling processes would likely be of the order of Z/c, it would

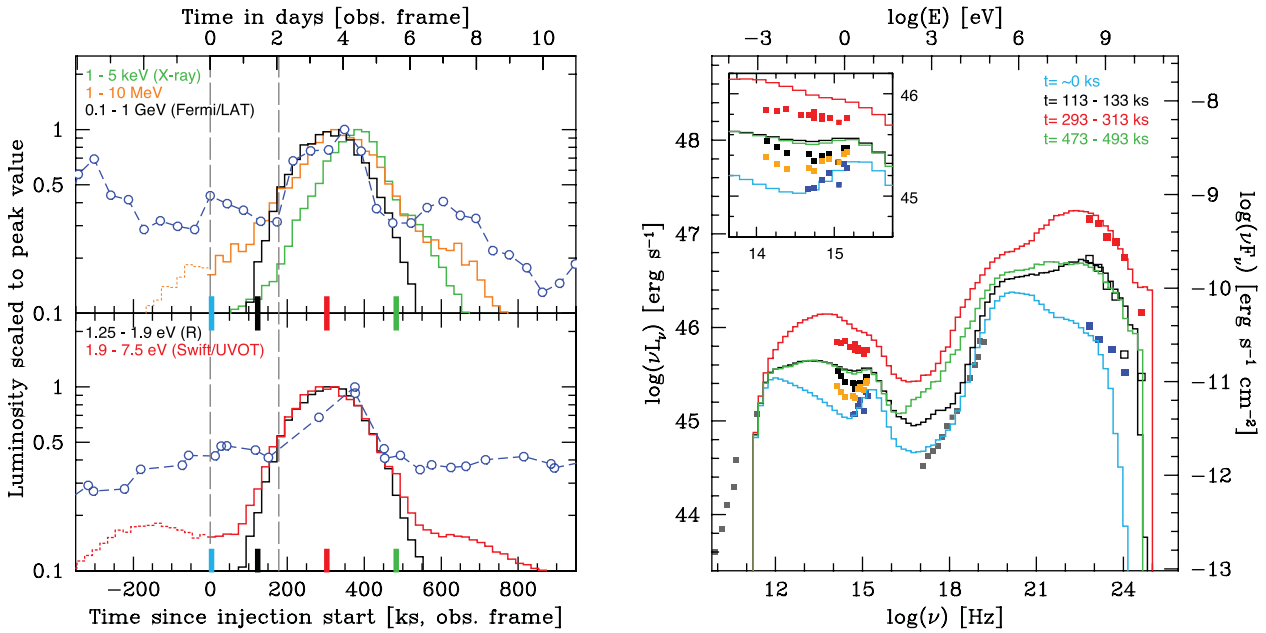

Figure 6. Light curves (left) and SEDs (right) for the case with the EC dominated by radiation from the torus. Parameters are listed in Table 1, `torus15`.

certainly be desirable to not be forced to such extreme values for $t'_{\rm esc}$, and we regard this as a serious problem for EC on torus emission, in the framework discussed here.

4.6 Pure SSC

We already cited some of the recent results suggesting that the active, γ-ray-emitting region in the jets of several blazars may be located beyond the size scale of the BLR on the basis of correlated multiwavelength variability and Very Long Baseline Array (VLBA) imaging (Larionov et al. 2008; Sikora, Moderski & Madejski 2008; Marscher et al. 2010; Agudo et al. 2011a,b).

Additionally, the detection in TeV γ-rays of a few FSRQs, including a recent confirmation for PKS 1510−089 (Cortina et al. 2012) (others are 3C 279, Albert et al. 2008; Aleksić et al. 2011a and PKS 1222+216, Aleksić et al. 2011b), challenges traditional EC scenarios because jet-emitted TeV photons would be readily lost by photon–photon pair production with the copious soft photons surrounding the jet. These findings have thus stimulated a renewed interest in the possibility that even for some of these powerful jets in systems with luminous accretion disc and broad-line emission, the γ-ray emission may be predominantly by SSC (for analysis on 3C 279 see e.g. Böttcher, Reimer & Marscher 2009).

Finally, studying a large sample of well-characterized blazars detected by *Fermi*/LAT and with an estimate of their jet intrinsic power, Meyer et al. (2012) find that, while for the highest jet power objects there is a clear collective sign of EC being the dominant mechanism for their γ-ray emission, the properties of the rest of the population are consistent with SSC.

Moreover, as discussed in the previous sections, our simulations of EC models for the type of flaring blob scenario presented here show large variability in X-ray which is inconsistent with the very robust observational finding of lack of significant variations even during the flaring phase, and which is caused by the SSC contribution. The existence of this latter is unavoidable, and our tests suggest that even mitigating its effect is not a trivial endeavour (Sections 4.3 and 4.4).

Therefore, it seems natural to want to test if we could reproduce the benchmark observations with a pure SSC scenario. The results are shown in Fig. 7.

The SSC model reproduces well several aspects of the observations. In particular, the amplitude of the flux variability and the spectral change in the X-ray band are overall much closer to what was observed. The *Fermi*/LAT band spectrum and intensity are also well matched. Because of the presence of the steady disc emission mostly contributing to the blue/UV flux, the flux in the *R* band varies less than the *Swift*/UVOT band.

However, the simulations produce an X-ray spectrum consistently harder than the one observed, mostly determined by the sharp 'cut-off' of the lower energy end of the electron distribution. The observed SED, namely the very hard X-ray spectrum, constrains this latter to a fairly high $\gamma_{\rm min}$, much larger than the values used in the EC cases. The simulated IR spectrum is also somewhat harder than the spectrum observed in the intermediate state. Finally, the frequency at which the synchrotron spectrum peaks tends to be too high, which is a consequence of the high $\gamma_{\rm min}$ required by the X-ray spectrum.

Since the SSC model has fewer free parameters than the EC model, they are more constrained than those in the EC models, and do not leave us much freedom for improving significantly on these issues.

5 DISCUSSION AND CONCLUSIONS

We have modelled multiwavelength variability produced in the jet of PKS 1510−089, with EC model involving external radiation from BLR or dusty molecular torus, as well as pure SSC model.

As discussed also by Tavecchio & Ghisellini (2008), the use of a realistic BLR spectrum seems indeed to be critical to model accurately the IC component, in particular its lower energy end which is observed in great detail in the X-ray band, thus providing a powerful diagnostic on model parameters. The results presented here, namely the challenging issue of the large X-ray variability caused by the SSC contribution, which has a distinctly different spectral

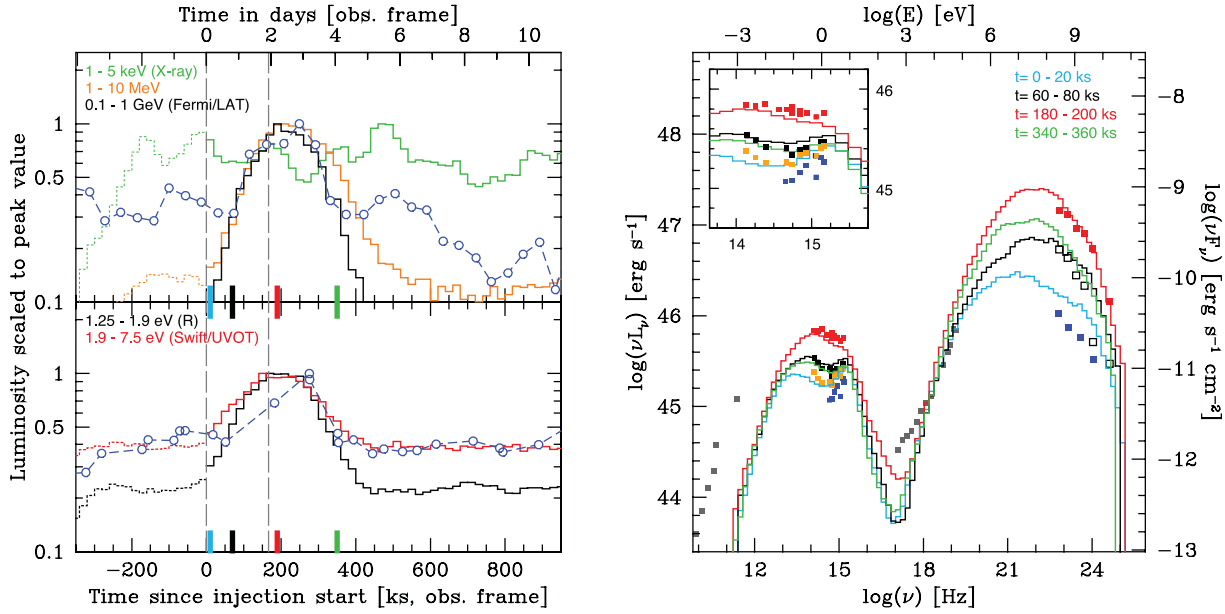

Figure 7. Light curves (left) and SEDs (right) for the SSC case. Parameters are listed in Table 1, ssc.

shape from the EC, further strengthen the importance of modelling as accurately as possible the source of the EC seed photons.

In the same context, we should comment on the fact, noted in Section 3.3, that in order to obtain reasonable SEDs and light curves in the EC/BLR cases we had to adopt a reprocessed fraction of BLR luminosity, $f_{\rm BLR}$, that is significantly smaller than what one would expect. A more traditional $f_{\rm BLR}$, such as 0.1 in Ghisellini & Tavecchio (2009), would yield a more intense BLR radiation energy density and the increased electron energy loss rate in the blob would push the model towards fairly extreme values for several of the parameters. This could be regarded as an indication that the general scenario that we studied in this work may not be a suitable explanation for flares in FSRQs. On the other hand, this scenario yields acceptable, though not perfect, results for the EC/torus and the SSC cases.

As discussed in Section 3.3, the combination of $(f_{\rm ext}\,\Gamma^2/R_{\rm ext}^2)/B^2$ is related to the ratio between the IC and the synchrotron luminosities (Compton dominance), which is an observable. Although its value may vary during a flare, the value of the Compton dominance imposes a relationship between those parameters of the source (hence model). A given source or source state may have a preferred value for the Compton dominance which should be matched by a combination of $f_{\rm ext}$, Γ and $R_{\rm ext}$ (and B), independently on whether one wants to model it with EC/BLR or EC/torus. For the Compton dominance ratio that seems to work well for PKS 1510−089, it is possible to adopt plausible values or $R_{\rm ext}$ and $f_{\rm ext}$ for the EC/torus case and less so for the EC/BLR case. This consideration does not depend strongly on the scenario adopted for the blob and the mechanism causing outbursts and it may suggest that indeed PKS 1510−089 may not be modelled by EC/BLR in general. Alternatively, it could mean that our naive idea of the BLR and torus does not represent their real structure and causes the EC/BLR model to fail to match the data. Another possibility is that the relativistic jet in this source has a milder bulk Lorentz factor Γ than 15 or 25 that we adopted in this paper. However, this in conflict with the high Γ required to avoid the large SSC contribution.

Leaving aside the above considerations, and looking at the results of the simulations as run with the best-fitting parameter sets, it is difficult to identify a clear superiority for any of them. None can be convincingly excluded.

The EC/BLR scenario suffers the problem of the large X-ray variability, and it produces better, marginally satisfactory, results if we adopt a larger value for the bulk Lorentz factor, which is still within the observed range. It also requires parameters for the BLR which are at least unusual.

The EC/torus also has the problem of highly variable SSC in the X-ray band, which we can expect to be mitigated by using a larger Lorentz factor, and it works with reasonable parameters for the external radiation component, but it requires very fast particle acceleration and escape time-scales to maintain the balance between acceleration and cooling for the high-energy electrons necessary to scatter to the GeV band the lower energy external photons.

The pure SSC model naturally addresses the X-ray variability issue, but at price of very high minimum electron energy to avoid significant emission in X-rays, which in turn make it difficult to reproduce the synchrotron peak region SED and makes the X-ray spectrum significantly harder than the observed one. Because its GeV emission comes from scattering lower energy photons than the EC/BLR case, like the EC/torus case the SSC requires fast escape time-scale, though less extreme, which could be considered a serious problem.

In all three cases, their X-ray problems may be relaxed if there is a slowly varying contribution from other emission regions, filling the dip between the synchrotron and IC components, softening the X-ray spectrum and diluting its variations.

Overall, while within the framework studied in this work we cannot firmly discriminate the three main scenarios, and the framework that we adopted is just one possibility, our results show clearly the differences produced by a more realistic treatment of the emitting source in the shape of SEDs and their time variability over relevant, observable time-scales.

These results demonstrate that proper modelling of the high-quality data produced by the plethora of best multiwavelength campaigns on the brightest *Fermi*/LAT blazars to exploit the wealth of information that they carry and advance our understanding of

their physics can only be achieved with time-dependent multizone simulations.

Looking forward, there are several aspects of the predicted source variability that we have not discussed, such as more detailed analysis of correlated variability (e.g. time lags). Moreover as shown here, SEDs exhibit complex features and variations and it may be possible to explain the interesting, challenging, observation of large break in the *Fermi*/LAT spectra seen in a handful of sources, comprising both FSRQs and low-peaked BL Lacs (Abdo et al. 2010a). The observed breaks are larger than what would be produced by cooling and too sharp to be consistent with an exponential cut-off. Several ideas have been proposed to explaining them as due to external factors, namely $\gamma\gamma$ absorption outside the jet (Ackermann et al. 2010; Finke & Dermer 2010; Poutanen & Stern 2010), and some are somewhat inconsistent with other multiwavelength properties.

Finally, in these simulations we have used a simple model of energy-independent particle acceleration, whereby in order to maintain a power-law electron distribution with a certain slope, the particle escape time-scale is tied to the acceleration time-scale. The fast radiative cooling in our model requires fast particle acceleration and hence fast particle escape. This required escape time-scale has turned out to be smaller than the limit of Z/c, which happens if all particles travel freely at the speed of light. However, the actual particle acceleration process is expected to have a more complicated energy dependence than assumed here. Therefore, the acceleration and escape time-scales derived here are only for instructive purposes. We will investigate whether a more realistic energy dependence of the particle acceleration process may change the required acceleration and escape time-scales.

ACKNOWLEDGMENTS

We would like to thank Fabrizio Tavecchio and Gabriele Ghisellini for providing their BLR spectra. This research has been supported by NASA grants NAG5-11796, NAG5-11853, NNX12AE43G, *Chandra* GO AR9-0016X and *Fermi* GI NNX10AO42G. MB acknowledges support by NASA through *Fermi* GI NNX10AU11G and ATP grant NNX10AC79G. This work was supported in part by the Shared University Grid at Rice funded by NSF under Grant EIA-0216467, and a partnership between Rice University, Sun Microsystems and Sigma Solutions, Inc. This work was supported in part by the Data Analysis and Visualization Cyberinfrastructure funded by NSF under grant OCI-0959097. This work was supported in part by the Cyberinfrastructure for Computational Research funded by NSF under Grant CNS-0821727. This research has made use of NASA's Astrophysics Data System and of the NASA/IPAC Extragalactic Database (NED) which is operated by the Jet Propulsion Laboratory, California Institute of Technology, under contract with the National Aeronautics and Space Administration.

REFERENCES

Abdo A. A. et al., 2009, ApJ, 699, 817
Abdo A. A. et al., 2010a, ApJ, 710, 1271
Abdo A. A. et al., 2010b, ApJ, 716, 835
Abdo A. A. et al., 2010c, ApJ, 721, 1425
Abramowski A. et al., 2012, A&A, 539, A149
Ackermann M. et al., 2010, ApJ, 721, 1383
Agudo I. et al., 2011a, ApJ, 726, L13
Agudo I. et al., 2011b, ApJ, 735, L10
Aharonian F. et al., 2007, ApJ, 664, L71
Albert J. et al., 2008, Sci, 320, 1752
Aleksić J. et al., 2011a, A&A, 530, A4
Aleksić J. et al., 2011b, ApJ, 730, L8
Arbeiter C., Pohl M., Schlickeiser R., 2005, ApJ, 627, 62
Bentz M. C., Peterson B. M., Pogge R. W., Vestergaard M., Onken C. A., 2006, ApJ, 644, 133
Bentz M. C., Peterson B. M., Netzer H., Pogge R. W., Vestergaard M., 2009, ApJ, 697, 160
Bonnoli G., Ghisellini G., Foschini L., Tavecchio F., Ghirlanda G., 2012, MNRAS, 410, 368
Böttcher M., 2007, Ap&SS, 309, 95
Böttcher M., Reimer A., Marscher A. P., 2009, ApJ, 703, 1168
Chen X., 2012, PhD thesis, Rice Univ.
Chen X., Fossati G., Liang E., Böttcher M., 2011a, JA&A, 32, 185
Chen X., Fossati G., Liang E. P., Böttcher M., 2011b, MNRAS, 416, 2368
Chiaberge M., Ghisellini G., 1999, MNRAS, 306, 551
Cortina J. et al., 2012, Astron. Telegram, 3965, 1
D'Ammando F. et al., 2011, A&A, 529, A145
Dermer C., Lott B., 2012, J. Phys. Conf. Ser., 355, 012010
Dermer C. D., Schlickeiser R., Mastichiadis A., 1992, A&A, 256, L27
Finke J. D., Dermer C. D., 2010, ApJ, 714, L303
Fossati G. et al., 2008, ApJ, 677, 906
Ghisellini G., Madau P., 1996, MNRAS, 280, 67
Ghisellini G., Tavecchio F., 2009, MNRAS, 397, 985
Graff P. B., Georganopoulos M., Perlman E. S., Kazanas D., 2008, ApJ, 689, 68
Hinton J. A., Hofmann W., 2009, ARA&A, 47, 523
Jorstad S. G. et al., 2005, AJ, 130, 1418
Kaspi S., Brandt W. N., Maoz D., Netzer H., Schneider D. P., Shemmer O., 2007, ApJ, 659, 997
Kataoka J., Takahashi T., Makino F., Inoue S., Madejski G. M., Tashiro M., Urry C. M., Kubo H., 2000, ApJ, 528, 243
Kataoka J. et al., 2008, ApJ, 672, 787
Katarzyński K., Ghisellini G., Mastichiadis A., Tavecchio F., Maraschi L., 2006, A&A, 453, 47
Katarzyński K., Lenain J., Zech A., Boisson C., Sol H., 2008, MNRAS, 390, 371
Larionov V. M. et al., 2008, A&A, 492, 389
Levinson A., 2006, Int. J. Modern Phys. A, 21, 6015
Malmrose M. P., Marscher A. P., Jorstad S. G., Nikutta R., Elitzur M., 2011, ApJ, 732, 116
Mannheim K., 1998, Sci, 279, 684
Marscher A. et al., 2010, ApJ, 710, L126
Meyer E. T., Fossati G., Georganopoulos M., Lister M. L., 2012, ApJ, 752, L4
Pier E. A., Krolik J. H., 1992a, ApJ, 399, L23
Pier E. A., Krolik J. H., 1992b, ApJ, 401, 99
Poutanen J., Stern B., 2010, ApJ, 717, L118
Pucella G. et al., 2008, A&A, 491, L21
Rachen J. P., 2000, in Dingus B. L., Salamon M. H., Kieda D. B., eds, AIP Conf. Proc. Vol. 515, GeV-TeV Gamma Ray Astrophysics Workshop: Towards a Major Atmospheric Cherenkov Detector VI. Am. Inst. Phys., New York, p. 41
Sikora M., Madejski G., 2001, in Aharonian F. A., Völk H. J., eds, AIP Conf. Ser. Vol. 558, High Energy Gamma-ray Astronomy: International Symposium. Am. Inst. Phys., New York, p. 275
Sikora M., Begelman M. C., Rees M. J., 1994, ApJ, 421, 153
Sikora M., Moderski R., Madejski G. M., 2008, ApJ, 675, 71
Sikora M., Stawarz Ł., Moderski R., Nalewajko K., Madejski G. M., 2009, ApJ, 704, 38
Sokolov A., Marscher A. P., 2005, ApJ, 629, 52
Sokolov A., Marscher A. P., McHardy I. M., 2004, ApJ, 613, 725
Tavecchio F., Ghisellini G., 2008, MNRAS, 386, 945
Thompson D. J., Djorgovski S., de Carvalho R., 1990, PASP, 102, 1235
Tramacere A., Massaro E., Taylor A. M., 2011, ApJ, 739, 66

This paper has been typeset from a TEX/LATEX file prepared by the author.